



THE UNIVERSITY *of* EDINBURGH

Edinburgh Research Explorer

Arctic warming-induced cold damage to East Asian terrestrial ecosystems

Citation for published version:

Kim, J-S, Kug, J-S, Jeong, S-J, Zhao, Y, Chen, X, Williams, M, Ichii, K & Schaeppman-Strub, G 2022, 'Arctic warming-induced cold damage to East Asian terrestrial ecosystems', *Communications Earth & Environment*, vol. 3, 16. <https://doi.org/10.1038/s43247-022-00343-7>

Digital Object Identifier (DOI):

[10.1038/s43247-022-00343-7](https://doi.org/10.1038/s43247-022-00343-7)

Link:

[Link to publication record in Edinburgh Research Explorer](#)

Document Version:

Publisher's PDF, also known as Version of record

Published In:

Communications Earth & Environment

Publisher Rights Statement:

© The Author(s) 2022

General rights








Copyright for the publications made accessible via the Edinburgh Research Explorer is retained by the author(s) and / or other copyright owners and it is a condition of accessing these publications that users recognise and abide by the legal requirements associated with these rights.

Take down policy

The University of Edinburgh has made every reasonable effort to ensure that Edinburgh Research Explorer content complies with UK legislation. If you believe that the public display of this file breaches copyright please contact openaccess@ed.ac.uk providing details, and we will remove access to the work immediately and investigate your claim.



Arctic warming-induced cold damage to East Asian terrestrial ecosystems

Jin-Soo Kim ¹, Jong-Seong Kug ^{2✉}, Sujong Jeong³, Jin-Ho Yoon⁴, Ning Zeng⁵, Jinkyu Hong ⁶, Jee-Hoon Jeong ⁷, Yuan Zhao⁸, Xiaoqiu Chen⁸, Mathew Williams ⁹, Kazuhito Ichii ¹⁰ & Gabriela Schaepman-Strub ¹

The global mean temperature is increasing due to the increase in greenhouse gases in the atmosphere, but paradoxically, many regions in the mid-latitudes have experienced cold winters recently. Here we analyse multiple observed and modelled datasets to evaluate links between Arctic temperature variation and cold damage in the East Asian terrestrial ecosystem. We find that winter warming over the Barents-Kara Sea has led to simultaneous negative temperature anomalies over most areas in East Asia and negative leaf area index anomalies in southern China where mostly subtropical evergreen forests are growing. In addition to these simultaneous impacts, spring vegetation activity and gross primary productivity were also reduced over evergreen and deciduous trees, and spring phenological dates are delayed. Earth System model simulations reveal that cold damage becomes stronger under greenhouse warming; therefore Arctic warming-induced cold stress should be considered in forest and carbon management strategies.

¹Department of Evolutionary Biology and Environmental Studies, University of Zurich, Zurich, Switzerland. ²Division of Environmental Science and Engineering, Pohang University of Science and Technology (POSTECH), Pohang, South Korea. ³Department of Environmental Planning, Graduate School of Environmental Studies, Seoul National University, Seoul, South Korea. ⁴School of Earth Sciences and Environmental Engineering, Gwangju Institute of Science and Technology, Gwangju, South Korea. ⁵Department of Atmospheric and Oceanic Science, University of Maryland, College Park, MD, USA. ⁶Department of Atmospheric Sciences, Yonsei University, Seoul, South Korea. ⁷Faculty of Earth and Environmental Sciences, Chonnam National University, Gwangju, South Korea. ⁸College of Urban and Environmental Sciences, Laboratory for Earth Surface Processes of the Ministry of Education, Peking University, Beijing, People's Republic of China. ⁹School of GeoSciences and National Centre for Earth Observation, University of Edinburgh, Edinburgh, UK. ¹⁰Center for Environmental Remote Sensing, Chiba University, Chiba, Japan. ✉email: jskug@postech.ac.kr

With average temperatures rising around the world due to greenhouse gas emissions, the Arctic shows stronger increasing temperature trends than other regions¹. This warming has been termed as the Arctic Amplification². At the same time, high-latitude greening is also observed due to rapid temperature increases^{3,4}. In contrast to this faster warming and enhanced vegetation cover and production across the Arctic, severe cold events can cause negative impacts on vegetation in the mid-latitudes, as documented for North America^{5–7}. There are two distinct relations of anomalous Arctic warming from the East Siberian–Chukchi and Barents–Kara sea regions with cold winters over North America and East Asia with downstream teleconnections, respectively⁸. Thereby it is likely that East Asia is also affected by Arctic warming-related cold damage on terrestrial ecosystem productivity because temperature variation during the cold season is a critical phenological factor for determining the start of the growing season⁹. As the terrestrial ecosystem is one of the most important components in the global carbon cycle¹⁰ and East Asia has undergone rapid economic growth and fossil fuel emission increases over the past decades, understanding Arctic warming-induced carbon balance changes in East Asian terrestrial ecosystems are necessary for preparing a carbon-neutral strategy¹¹.

Results

Atmospheric teleconnections linked to Arctic warming. The Arctic Temperature (ART) index⁸ is defined as de-trended surface temperature anomalies, during boreal winter (December–February) over the Barents–Kara Sea (160°E–160°W, 65°–80°N), where pronounced sea ice reduction and temperature increase were observed in recent decades, to examine relevant teleconnection patterns and impacts on East Asian vegetation activity (Fig. 1c). The regressed low-level circulation pattern onto the ART index clearly shows anticyclonic flow centered on interior Siberia that is slightly southeastward shifted from the Barents–Kara Sea (Fig. 1a). In contrast to the positive temperature anomalies in northwestern and northeastern Siberia, many countries in the Middle East and East Asia have significantly negative temperature anomalies, such as Iran, Afghanistan, Turkmenistan, Uzbekistan, Mongolia, China, South and North Korea, and Japan, except for the Tibetan Plateau. This dipole temperature pattern during boreal winter is pointed out in literature as the warm Arctic and cold Eurasia (WACE) pattern that induces stronger East Asia winter monsoon and cold events due to intensified and westward shifted Asian trough teleconnection to Barents–Kara Sea warming¹². The anticyclonic system around the high-latitude has a vertically barotropic structure and a cyclonic circulation is developed in the mid-latitude downstream region via Rossby wave energy propagation^{13,14} with negative temperature anomalies even in subtropical regions down to around 20°N, but the Rossby wave trains do not propagate further when they encounter the Tibetan Plateau (Fig. 1c and Supplementary Fig. 1). Mongolia, southern China, and the Korean Peninsula particularly have strong negative temperature anomalies due to northerly wind which is directed parallel to isobars (Supplementary Fig. 2).

Vegetation activity anomalies linked to Arctic warming. With negative winter surface temperature anomalies over East Asia related to the ART index (Fig. 2a), relevant negative leaf area index (LAI) anomalies were observed in southern China during boreal winter (Fig. 2c). While deciduous trees in temperate latitudes generally are in a dormant stage during boreal winter, southern China is composed of tropical and subtropical evergreen forests and local temperature variation is an important driver of vegetation activity there^{15,16} (Fig. 2e). For example, an extreme ice storm struck southern and central China in early 2008¹⁷, also

marked as one of the positive Arctic warming years in Fig. 1c, and approximately 13% of Chinese forests were damaged during this ice-snow disaster due to both physical and physiological damages such as bending, breakage, splitting, cold injury and mortality^{17,19}. We found that averaged surface temperature and LAI anomalies were -1.19°C and $-0.15\text{ m}^2\text{ m}^{-2}$ over southern China (110°–120°E, 20°–30°N), which represents a reduction of LAI of -9.7% compared to the climatological LAI, in composites of Arctic warming years that are 1983, 1984, 2005, 2008, 2012, and 2016 (Fig. 1c, also Supplementary Fig. 3). On the other hand, negative LAI anomalies are also detected in southwestern Japan which has substantial evergreen needle leaf forests (Fig. 2f), but these are relatively weaker because temperature anomalies are weak and needle leaf species have stronger resistance to winter chilling than broadleaf species²⁰.

Even though winter LAI anomalies in other East Asia regions, except for southern China, are negligible due to limited vegetation activity in winter, it is striking that LAI is significantly reduced in boreal spring (March–May) over many areas of East Asia, such as southern China, northeastern China, the Korean Peninsula, and Japan, related to the winter ART index (Fig. 2d). Springtime temperature anomalies are generally weak and nonsignificant except for some areas in southeastern China and Japan, however, significant LAI anomalies are extensively detected in not only evergreen but also deciduous forests over East Asia (Fig. 2g). This is consistent with previous studies that argued temperature variation in the pre-season, such as winter chilling, to be a critical factor of spring phenology^{21–23}. While local temperature anomalies in spring are weaker and nonsignificant than anomalies in winter, LAI anomalies can be significant due to the high sensitivity of LAI to temperature and significant negative temperature anomalies in the pre-season such as February–April (Supplementary Fig. 4). Separating the contribution of spring LAI anomalies reveals that local winter temperature variation plays a substantial role in spring LAI anomalies not only for evergreen forests in southern China and Japan but also for deciduous forests in northeastern China and Korean Peninsula (Supplementary Fig. 5). Thus, Arctic warming-related winter chilling simultaneously reduces winter vegetation activity in East Asian evergreen forests and also in spring phenology due to lagged impacts from temperature variation in winter.

Consistently with the present analysis based on the observed dataset, offline Land Surface Model (LSM) results also show significant negative LAI anomalies in winter and spring related to the ART index (Supplementary Fig. 6). Even though spatial patterns and magnitude in LAI anomalies are diverse among LSMs, simulated winter LAI anomalies have strong negative patterns over southern China, but not for other regions, which might be due to the lack of vegetation activity in winter (similar to Fig. 2c). Significant spring LAI anomalies over southern and northeastern China, the Korean Peninsula, and Japan were also detected, which supports our hypothesis that winter chilling from anomalous Arctic warming affects spring vegetation activity. This might result in LSMs often prescribing the start of growing season or tree mortality rate based on threshold temperatures depending on Plant Functional Types (PFTs)²⁴. In detail, the LSM of IPSL-CM6A-LR employs specific schemes for simulating cold damages that are tree mortality due to extremely cold days and tree extension limits by growing season temperature²⁵. Also, this model evaluation showed good agreement (low bias) with the timing of the growing season over East Asia²⁶.

To examine the role of winter and spring temperature variation on spring LAI, we conduct LSM experiments based on Vegetation-Global-Atmosphere-Soil (VEGAS)²⁷ and the Community Land Model, Version 5 (CLM5)²⁸ by prescribing climatological temperature in winter and spring. Simulated

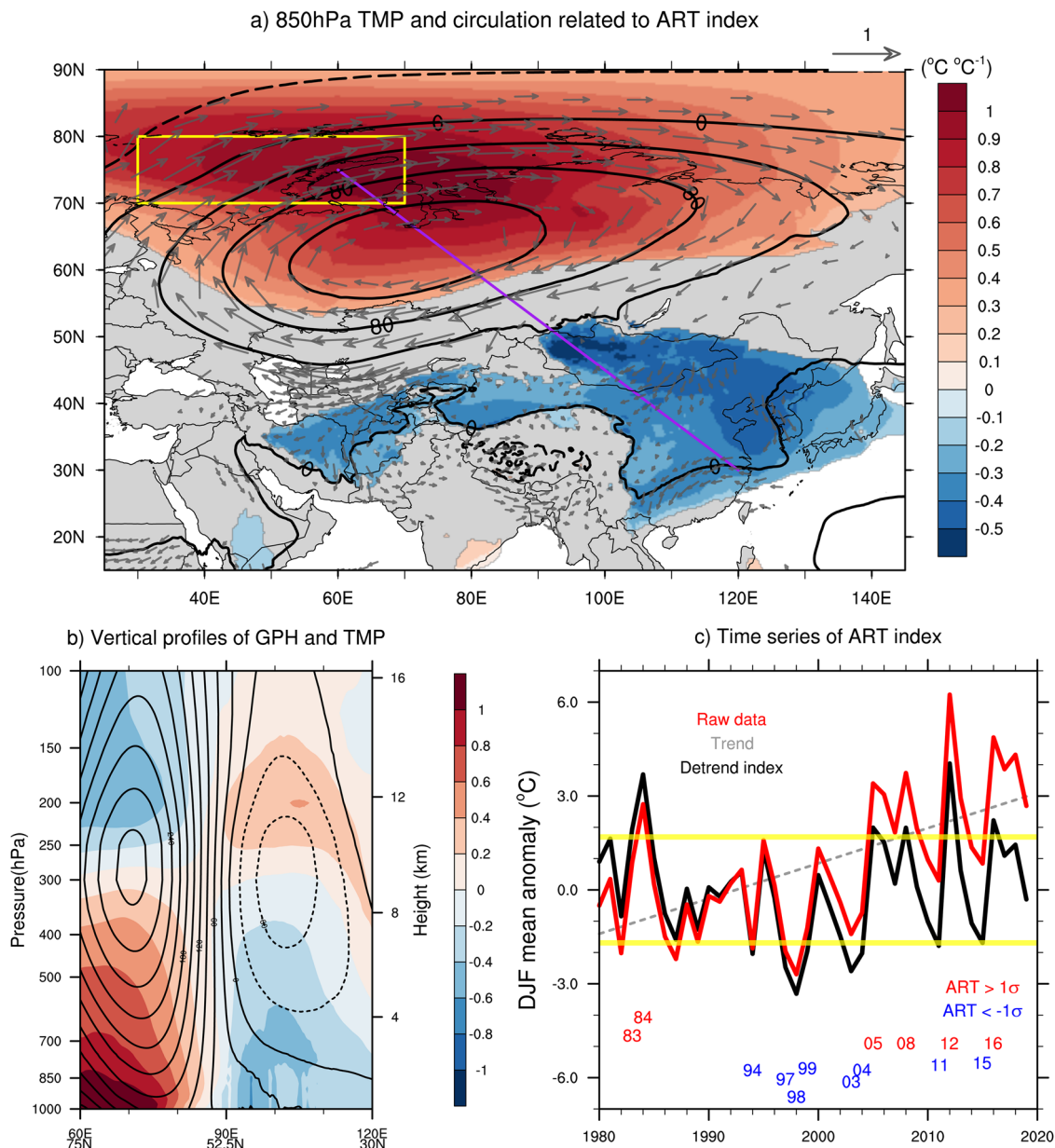


Fig. 1 Barents-Kara Sea temperature variability and relevant teleconnection. **a** Regression coefficients of December–February averaged 2-meter temperature ($^{\circ}\text{C } ^{\circ}\text{C}^{-1}$), 850-hPa geopotential height ($\text{m } ^{\circ}\text{C}^{-1}$), and wind ($\text{m s}^{-1} ^{\circ}\text{C}^{-1}$) onto de-trended Barents-Kara Sea (yellow box; 30° – 70°E , 70° – 80°N) temperature anomaly (ART index). Wind vectors and shading are displayed only in significant regions at the 95% confidence level (calculated using a Student’s *t*-test). **b** Time series of raw ART index and de-trended index. Yellow lines show $\pm 1\sigma$ and Arctic warming ($>1\sigma$) and cooling ($<-1\sigma$) years are marked. **c**, Regression coefficients of vertical profiles of geopotential height (m; contour) and temperature ($^{\circ}\text{C}$, shaded) from 1000-hPa to 100-hPa along 60°E , 75°N – 120°E , 30°N (the diagonal purple line in **a**).

ART-related LAI anomalies with winter climatological temperature have weaker magnitude than the control experiments, while the experiment result with fixed spring temperature has a similar spatial pattern and magnitude of LAI anomalies (Supplementary Figs. 7, 8). These results might be driven from the cold mortality scheme; VEGAS has exponential increases of cold stress mortality with temperature decreases less than 5°C and CLM5 has a phenology scheme with an onset trigger based on an accumulated growing-degree-day approach²⁹. However, neither model is sensitive to the low-temperature impact on needle leaf forests, such as physical damages by frozen rain and heavy snow events^{17–19}, which leads to underestimation of reduced LAI from winter chilling over East Asia.

Delayed spring phenology linked to Arctic warming. In addition to LAI data based on remote sensing and offline modelling, in-situ observations of spring phenology datasets over southern and northeastern China, South Korea, and Japan were analysed to find a linkage between Arctic warming-induced spring phenological date changes. Observed budburst, first and peak flower dates at many in-situ stations show significant positive relationships with the ART index (Fig. 3). In southern China, all observation dates of first leaf unfolding, 50% leaf unfolding and the end flowering show delayed phenological dates with anomalous Arctic warming³⁰ (Supplementary Fig. 9). The first flowering date, which has the fewest missing observations, was observed for many species and shows significant results ($P < 0.05$) across

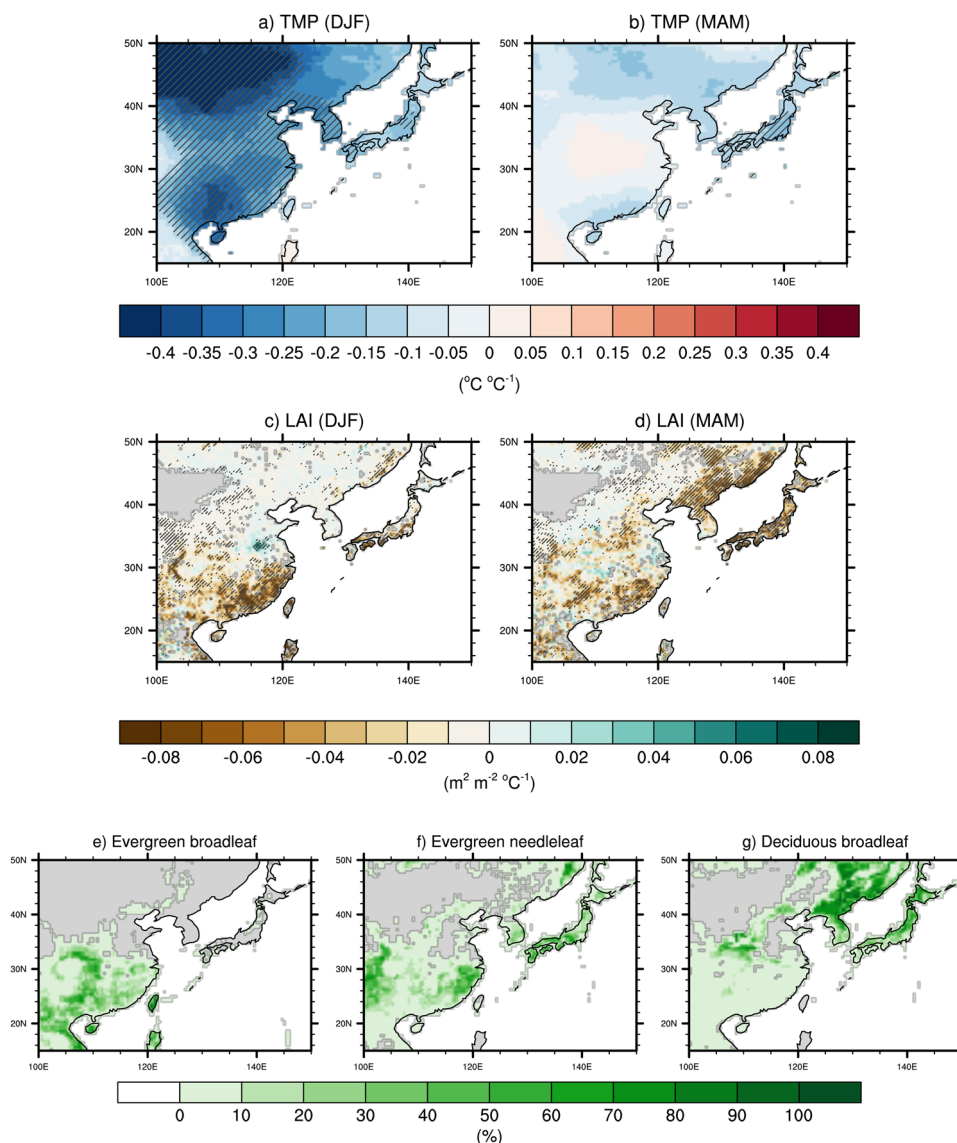


Fig. 2 Temperature and leaf area index anomaly related to Arctic warming. **a–d** Regression coefficients of seasonal mean temperature ($^{\circ}\text{C } ^{\circ}\text{C}^{-1}$) (**a, b**) and leaf area index anomaly ($\text{m}^2 \text{m}^{-2} \text{ } ^{\circ}\text{C}^{-1}$) (**c, d**) during boreal winter (December–February) (**a, c**) and spring (March–May) (**b, d**) onto December–February ART index. Hatching indicates significant regions at the 95% confidence level based on the Student’s *t*-test. **e–g** Land cover type fractions (%) of evergreen broadleaf (**e**), evergreen needleleaf (**f**) and deciduous broadleaf (**g**).

several sites, such as 17 sites of *Melia azedarach* in southern China and 27 sites of *Prunus jamasakura* over South Korea and at 72 sites over Japan (Supplementary Table 1). The maximum differences for first flower date observations in each country between Arctic warming ($\text{ART} > 1\sigma$) and cooling years ($\text{ART} < -1\sigma$) are 20 days for *Platycladus orientalis* in Xuancheng (China), 15 days for *Forsythia koreana* in Jinju (South Korea) and 43 days for *Camellia japonica Linnaeus* in Tsu (Japan). Our results are consistent with previous studies that colder winter temperatures result in later flowering^{31,32}, but we additionally found a remote linkage between anomalous Arctic warming and phenology delays in East Asia.

Intensified vegetation impacts on Arctic warming under greenhouse warming. 21 Earth System models (ESM) in the Coupled Model Intercomparison Project Phase 6 (CMIP6) represent Arctic warming-related negative temperature anomalies and Rossby wave energy propagation from Barents-Kara Sea to

East Asia which is already reported based on the CMIP5³³ (Fig. 4; Supplementary Fig. 10). Spring LAI anomalies related to ART index show negative patterns similar to observational and offline model results, but magnitudes of LAI anomalies are weak due to weaker Arctic warming-induced winter cooling³⁴. In addition, we found an intensified Arctic-to-extratropical teleconnection over East Asia under greenhouse warming scenarios in the CMIP6. Vertical structures of geopotential height and temperature field are intensified, indicating stronger Rossby wave propagation in the upper layer of the atmosphere that might be due to the weakening of the vertical temperature gradient by Arctic surface warming³⁵ (Fig. 4c), and winter temperature teleconnections are also intensified (Fig. 4f). As a result, the spring LAI anomalies associated with the winter Arctic warming are intensified under greenhouse warming (Fig. 4i and Supplementary Fig. 11). This result implies that cold damage in the terrestrial ecosystem would continue to persist and even intensify in a warmer climate. Moreover, previous studies argued enhanced phenological frost

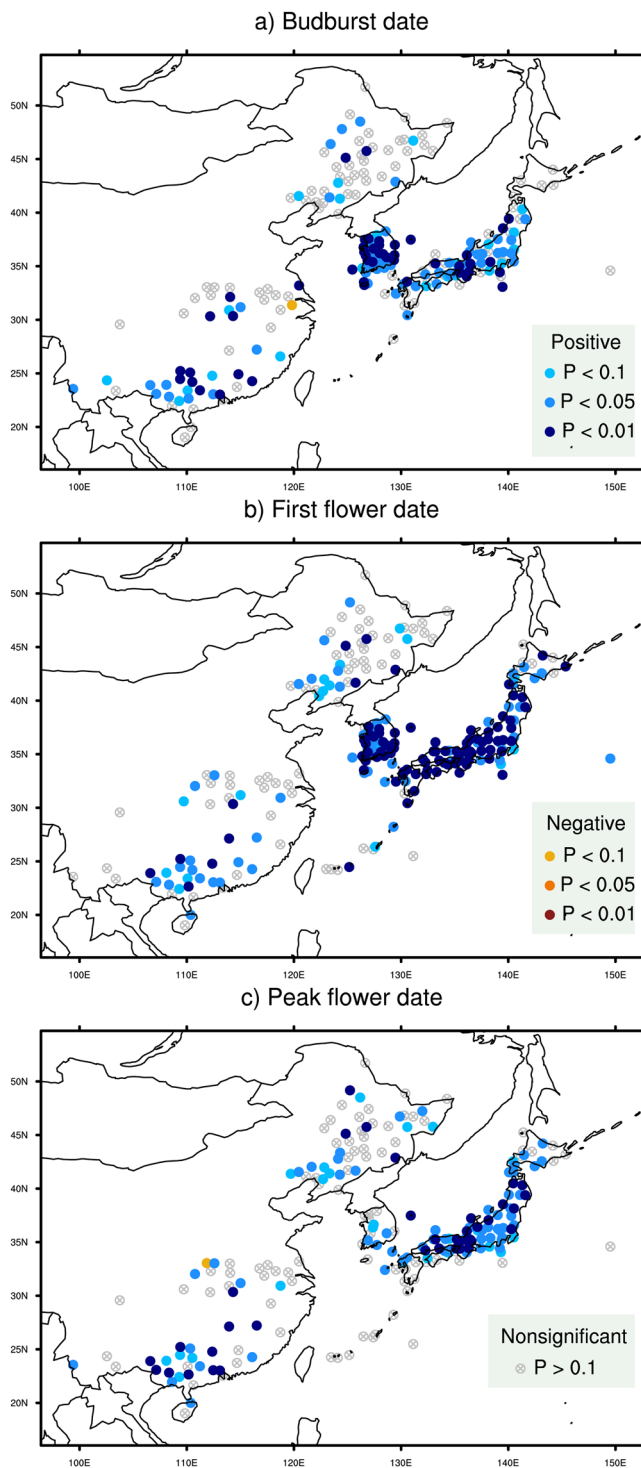


Fig. 3 Delayed phenological dates related to Arctic warming. a–c Statistical confidence based on correlation coefficient between December–February averaged ART index and in-situ phenological dates observation for budburst (a), first flower (b) and peak flower dates (c) based on Student’s *t*-test. Blue dots indicate delayed phenological dates and red dots earlier phenological dates onto December–February ART index.

damage in a warming climate due to the earlier start of the growing season with global warming^{7,36–38}, thereby an intensified Arctic-induced teleconnection might bring severe cold damage in the future.

Discussion

Overall, the present study demonstrates a lagged linkage between winter Arctic temperature variations and spring vegetation activity across East Asia from subtropical to boreal forests, while the ref 7. shows simultaneous terrestrial response only in spring. This linkage could be useful to forecast vegetation activity and ensure crop and forest productivity. Even though datasets of gross primary production (GPP) are only available since 2001, two independent data-driven GPP datasets reveal that estimated total GPP anomalies over East Asia (100°–150°E, 15°–50°N) are -65.91 and -67.15 TgC in winter and spring of Arctic warming years ($ART > 1\sigma$)^{39,40} (Supplementary Fig. 12). The minimum negative GPP anomaly over southern China (110°–120°E, 20°–30°N) in winter is up to -14.9% and -18.3% for spring as compared to the climatological value, over northern China, the Korean Peninsula and Japan region (120°–150°E, 30°–50°N). These results imply that Arctic warming-induced cold damages should be accounted for in terrestrial CO₂ sequestration and carbon balance estimates. Afforestation in southern China strongly plays a role in the sink of CO₂¹¹, but it should be monitored because younger trees are more susceptible to cold damage. We also found significant negative relationships between ART index and crop yields such as cereals, fruits, root vegetables, pulses, and nuts (Supplementary Table 2), thereby we conclude that anomalous Arctic warming has negative impacts on socio-economic factors not only directly linked to adverse weather conditions but also in agricultural productivity over East Asia.

Methods

Arctic temperature index (ART). We define the ART index as the de-trended surface temperature anomaly during December–February by averaging over the Barent–Kara Sea (30°–70°E, 70°–80°N) on the basis of the observations derived from interpolated HadCRUT4 data hybridized with the University of Alabama in Huntsville satellite data⁴¹ for the period 1979–2019.

Used dataset to obtain ART-induced teleconnection. To estimate the ART-induced teleconnection pattern, data on the temperature, geopotential height, and wind on pressure levels for the period 1979–2019 are obtained from the ERA5 (European Centre for Medium-Range Weather Forecasts Reanalysis)⁴² monthly surface temperature and precipitation are quantified using Climatic Research Unit (CRU) TS4.04 for the period 1979–2019⁴³.

Several data sets are used to obtain a robust relation between the ART index and vegetation activity anomalies (Supplementary Table 3). The Leaf Area Index data is the product of the Global Inventory Modeling and Mapping Studies (GIMMS) database, obtained from the Advanced Very High-Resolution Radiometer (AVHRR) remote-sensed observations⁴⁴. The 8-km grids were re-gridded to a common $0.5^\circ \times 0.5^\circ$ latitude/longitude grid for the period 1981–2016. The land cover data layer was obtained from the ESA GlobCover map⁴⁵ and was re-gridded to a common $0.5^\circ \times 0.5^\circ$ latitude/longitude grid.

To examine anomalous Arctic warming impacts on spring phenology, phenology dates over Korea and Japan were downloaded for the period 1979–2019 from the data portal of the Korea Meteorological Administration according to Korea Open Government License (KOGL) and Japan Meteorological Agency (<http://www.data.jma.go.jp/sakura/data/index.html>). Phenological datasets over China were provided by the meteorological information center of the China Meteorological Administration (CMA).

Furthermore, the relationship between the ART index and relevant impacts is investigated in each of the 21 coupled Earth System Models incorporated in the Coupled Model Intercomparison Project Phase 6^{46,47}. We use the data for the pre-industrial, historical, and Shared socioeconomic Pathway 5-8.5 scenarios in each model and re-gridded results into a common $1^\circ \times 1^\circ$ latitude/longitude grid. Details of each model are listed in Supplementary Table 4.

Land surface model experiments. Vegetation–Global–Atmosphere–Soil (VEGAS)²⁷ and the Community Land Model, Version 5 (CLM5)²⁸ are employed to investigate the role of winter temperature on spring LAI anomalies over East Asia. The control experiment is performed based on the Global Soil Wetness Project version 3 (GSWP3)⁴⁸ for the period 1979–2014. Climatological mean values of winter temperature (December–February) in each grid are prescribed to perform the “DJF-fix” experiment and the “MAM-fix” experiment which is prescribed climatological temperature for spring (March–May). Except for the corresponding temperature in each experiment, other input datasets are prescribed the same as control experiments.

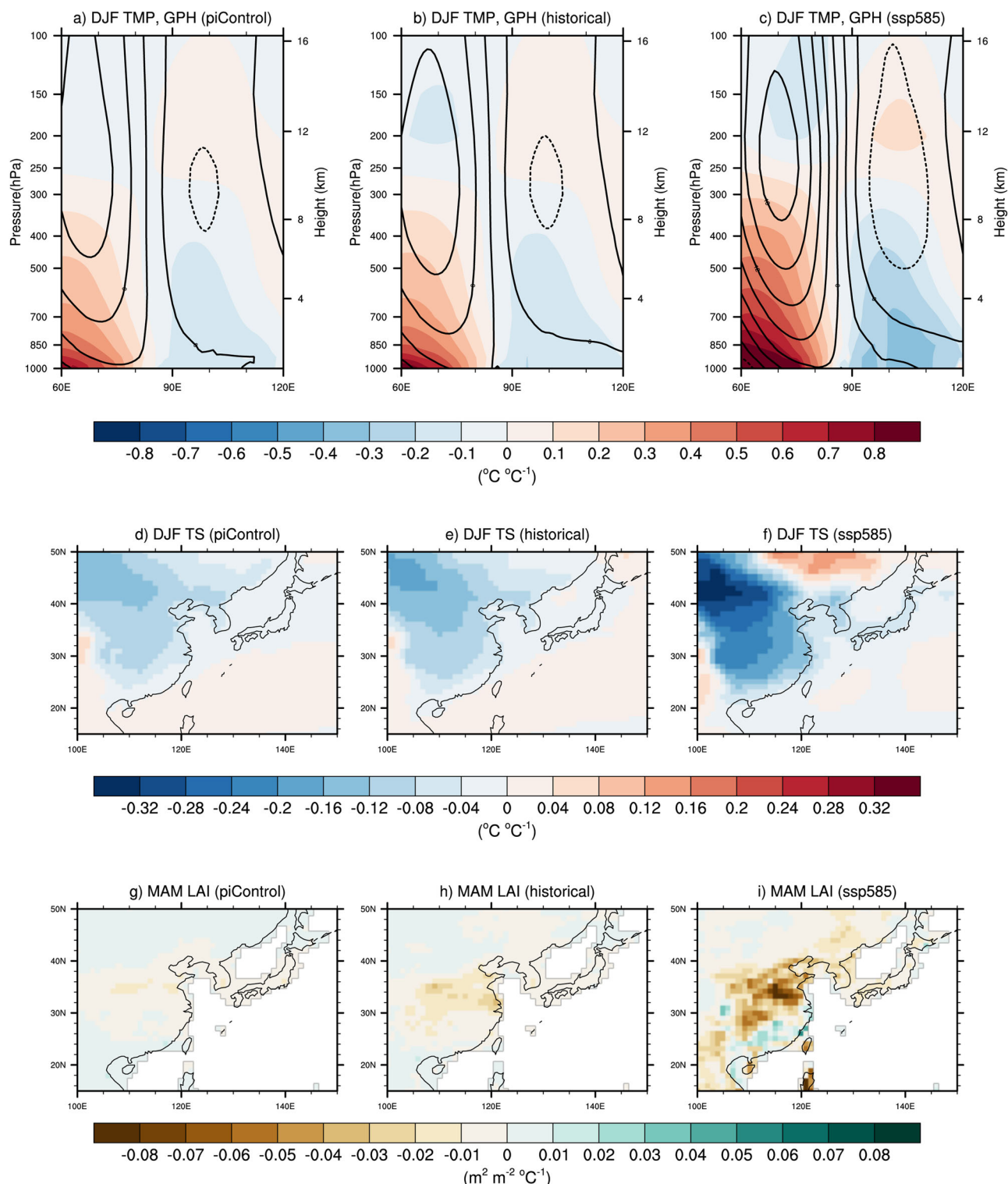


Fig. 4 Intensified Arctic warming-related teleconnections. **a–i** The CMIP6 Multi-model ensembles of regression coefficients of December–February averaged geopotential height ($\text{m } ^\circ\text{C}^{-1}$; contour) and temperature ($^\circ\text{C } ^\circ\text{C}^{-1}$, shaded) (**a–c**), December–February averaged temperature ($^\circ\text{C } ^\circ\text{C}^{-1}$) (**d–f**), and March–May averaged leaf area index anomaly ($\text{m}^2 \text{m}^{-2} ^\circ\text{C}^{-1}$) (**g–i**) onto December–February ART index under pre-industrial (**a, d, g**), historical (**b, e, h**), and ssp585 (**c, f, i**) scenarios.

Linear regression analysis. Linear regression is conducted to estimate the ART-induced teleconnection and terrestrial impacts onto the de-trended ART index. In order to focus on interannual relation, linear trends from all datasets were firstly removed and the linear trend of ART index is accordingly removed based on the same data period of the target data. The significance test conducted in this study is based on a standard two-tailed Student's *t*-test. We also employed a field significance test based on 1000 Monte Carlo simulations to evaluate the significance of

LAI regression fields^{49,50}. The number of grids at the 95% confidence level rank 960th and 984th highest values among 1000, therefore the hypothesis is that the regression patterns in Fig. 2c,d are a chance occurrence that can be rejected at the 95% confidence level. As shown in Supplementary Fig. 5 and described in Supplementary Note 1, we also use a multiple regression to investigate the individual contributions of the temperature and precipitation anomalies to leaf area index^{51,52}. Consequently, the partial regression coefficients approximately

represent the sensitivities of leaf area index to surface temperature and precipitation. The data analysis was carried out using NCAR Command Language (NCL) Version 6.6.2.

Data availability

All data used in this study are publicly available and can be downloaded from the corresponding websites (HadCRUT4: <https://www-users.york.ac.uk/kdc3/papers/coverage2013/series.html>; ERA5; CRU; GIMMS LAI; GlobCover map: <http://maps.elie.ucl.ac.be/CCI/viewer/download.php>; Korean phenological date: <https://data.kma.go.kr/data/seasonObs/seasonObsDataList.do>; Japan phenological date: <http://www.data.jma.go.jp/sakura/data/index.html>; CMIP6). The other data used in this study are available from a persistent repository (<https://doi.org/10.6084/m9.figshare.16807012>).

Code availability

Code (<https://doi.org/10.6084/m9.figshare.16807018.v1>) that support the findings of the study are available in a persistent repository (<http://figshare.com>). The scripts for generating figures are available from J.-S.Kim upon request.

Received: 3 July 2021; Accepted: 6 January 2022;

Published online: 01 February 2022

References

- Post, E. et al. The polar regions in a 2 °C warmer world. *Sci. Adv.* **5**, eaaw9883 (2019).
- Arrhenius, S. On the influence of carbonic acid in the air upon the temperature of the ground. *London, Edinburgh, Dublin Phil. Mag. J. Sci.* **41**, 237–276 (1896).
- Myneni, R. B., Keeling, C. D., Tucker, C. J., Asrar, G. & Nemani, R. R. Increased plant growth in the northern high latitudes from 1981 to 1991. *Nature* **386**, 698–702 (1997).
- Bhatt, U. S. et al. Circumpolar Arctic tundra vegetation change is linked to sea ice decline. *Earth Intract* **14**, 1–20 (2010).
- Francis, J. A. & Vavrus, S. J. Evidence linking Arctic amplification to extreme weather in mid-latitudes. *Geophys. Res. Lett.* **39**, L06801 (2012).
- Cohen, J. et al. Recent Arctic amplification and extreme mid-latitude weather. *Nat. Geosci.* **7**, 627–637 (2014).
- Kim, J.-S. et al. Reduced North American terrestrial primary productivity linked to anomalous Arctic warming. *Nat. Geosci.* **10**, 572–576 (2017).
- Kug, J. S. et al. Two distinct influences of Arctic warming on cold winters over North America and East Asia. *Nat. Geosci.* **8**, 759–762 (2015).
- Jeong, S. J., Medvigy, D., Shevliakova, E. & Malyshev, S. Uncertainties in terrestrial carbon budgets related to spring phenology. *J. Geophys. Res.* **117**, G01030 (2012).
- Friedlingstein, P. et al. Global carbon budget 2020. *Earth Syst. Sci. Data* **12**, 3269–3340 (2020).
- Piao, S. L. et al. The carbon budget of terrestrial ecosystems in East Asia over the last two decades. *Biogeosciences* **9**, 3571–3586 (2012).
- Mori, M., Watanabe, M., Shiogama, H., Inoue, J. & Kimoto, M. Robust Arctic sea-ice influence on the frequent Eurasian cold winters in past decades. *Nat. Geosci.* **7**, 869–873 (2014).
- Takaya, K. & Nakamura, H. Mechanisms of intraseasonal amplification of the cold Siberian high. *J. Atmos. Sci.* **62**, 4423–4440 (2005).
- Honda, M., Inoue, J. & Yamane, S. Influence of low Arctic sea-ice minima on anomalously cold Eurasian winters. *Geophys. Res. Lett.* **36**, L08707 (2009).
- Piao, S. L. et al. Interannual variations of monthly and seasonal normalized difference vegetation index (NDVI) in China from 1982 to 1999. *J. Geophys. Res.* **108**, D144401 (2003).
- Hua, W. et al. Observational quantification of climatic and human influences on vegetation greening in China. *Remote Sens* **9**, 425 (2017).
- Zhou, B., Gu, L., Ding, Y. & Shao, L. The great 2008 Chinese ice storm: its socioeconomic–ecological impact and sustainability lessons learned. *Bull. Am. Meteorol. Soc.* **92**, 47–60 (2011).
- Shao, Q., Huang, L., Liu, J., Kuang, W. & Li, J. Analysis of forest damage caused by the snow and ice chaos along a transect across southern China in spring 2008. *J. Geogr. Sci.* **21**, 219–234 (2011).
- Wang, X., Huang, S., Li, J., Zhou, G. & Shi, L. Sprouting response of an evergreen broad-leaved forest to a 2008 winter storm in Nanling Mountains, southern China. *Ecosphere* **7**, e01395 (2016).
- Woodward, F. I. & Williams, B. G. Climate and plant distribution at global and local scales. *Vegetatio* **69**, 189–197 (1987).
- Menzel, A. et al. European phenological response to climate change matches the warming pattern. *Glob. Change Biol.* **12**, 1969–1976 (2006).
- Piao, S. L., Fang, J. Y., Zhou, L. M., Ciais, P. & Zhu, B. Variations in satellite-derived phenology in China's temperate vegetation. *Glob. Change Biol.* **12**, 672–685 (2006).
- Cook, B. I., Wolkovich, E. M. & Parmesan, C. Divergent responses to spring and winter warming drive community level flowering trends. *Proc. Natl Acad. Sci. USA* **109**, 9000–9005 (2012).
- Smith, B., Prentice, I. C. & Sykes, M. T. Representation of vegetation dynamics in the modelling of terrestrial ecosystems: comparing two contrasting approaches within European climate space. *Glob. Ecol. Biogeogr.* **10**, 621–637 (2001).
- Zhu, D. et al. Improving the dynamics of Northern Hemisphere high-latitude vegetation in the ORCHIDEE ecosystem model. *Geosci. Model Dev.* **8**, 2263–2283 (2015).
- Peano, D. et al. Plant phenology evaluation of CRESCENDO land surface models – Part 1: Start and end of the growing season. *Biogeosciences* **18**, 2405–2428 (2021).
- Zeng, N., Mariotti, A. & Wetzzel, P. Terrestrial mechanisms of interannual CO₂ variability. *Glob. Biogeochem. Cycles* **19**, GB1016 (2005).
- Lawrence, D. M. et al. The community land model version 5: description of new features, benchmarking, and impact of forcing uncertainty. *J. Adv. Model. Earth Syst.* **11**, 4245–4287 (2019).
- White, M. A., Thornton, P. E. & Running, S. W. A continental phenology model for monitoring vegetation responses to interannual climatic variability. *Glob. Biogeochem. Cycles* **11**, 217–234 (1997).
- Chen, X. Q., Wang, L. X. & Inouye, D. Delayed response of spring phenology to global warming in subtropics and tropics. *Agric. For. Meteorol.* **234–235**, 222–235 (2017).
- Aono, Y. & Kazui, K. Phenological data series of cherry tree flowering in Kyoto, Japan, and its application to reconstruction of springtime temperatures since the 9th century. *Int. J. Climatol.* **914**, 905–914 (2008).
- Pearse, W. D., Davis, C. C., Inouye, D. W., Primack, R. B. & Davies, T. J. A statistical estimator for determining the limits of contemporary and historic phenology. *Nat. Ecol. Evol.* **1**, 1876–1882 (2017).
- Jang, Y. S., Kug, J. S. & Kim, B. M. How well do current climate models simulate the linkage between Arctic warming and extratropical cold winters? *Clim. Dyn.* **53**, 4005–4018 (2019).
- Park, H. & Jeong, S. J. Leaf area index in Earth system models: how the key variable of vegetation seasonality works in climate projections. *Environ. Res. Lett.* **16**, 034027 (2021).
- Alexeev, V. A., Esau, I. N., Polyakov, I. V., Byam, S. J. & Sorokina, S. Vertical structure of recent Arctic warming from observed data and reanalysis products. *Climatic Change* **111**, 215–239 (2011).
- Hänninen, H. Climate warming and the risk of frost damage to boreal forest trees: identification of critical ecophysiological traits. *Tree Physiol* **26**, 889–898 (2006).
- Augsburger, C. K. Spring 2007 warmth and frost: phenology, damage and refoliation in a temperate deciduous forest. *Funct. Ecol.* **23**, 1031–1039 (2009).
- Liu, Q. et al. Extension of the growing season increases vegetation exposure to frost. *Nat. Commun.* **9**, 426 (2018).
- Ichii, K. et al. New data-driven estimation of terrestrial CO₂ fluxes in Asia using a standardized database of eddy covariance measurements, remote sensing data, and support vector regression. *J. Geophys. Res. Biogeosci.* **122**, 767–795 (2017).
- Li, X. & Xiao, J. A global, 0.05-degree product of solar-induced chlorophyll fluorescence derived from OCO-2, MODIS, and reanalysis data. *Remote Sens* **11**, 517 (2019).
- Cowtan, K. & Way, R. G. Coverage bias in the HadCRUT4 temperature series and its impact on recent temperature trends. *Q. J. R. Meteorol. Soc.* **140**, 1935–1944 (2014).
- Hersbach, H. et al. The ERA5 global reanalysis. *Q. J. R. Meteorol. Soc.* **146**, 1999–2049 (2020).
- Harris, I., Osborn, T. J., Jones, P. & Lister, D. Version 4 of the CRU TS monthly high-resolution gridded multivariate climate dataset. *Sci. Data* **7**, 109 (2020).
- Zhu, Z. et al. Global data sets of vegetation leaf area index (LAI) 3g and fraction of photosynthetically active radiation (FPAR) 3g derived from global inventory modeling and mapping studies (GIMMS) normalized difference vegetation index (NDVI3g) for the period 1981 to 2011. *Remote Sens.* **5**, 927–948 (2013).
- Bontemps, S. et al. Consistent global land cover maps for climate modeling communities: current achievements of the ESA's land cover CCI. In *ESA Living Planet Symp. 2013 CCI-4* (ESA, 2013).
- Eyring, V. et al. Overview of the Coupled Model Intercomparison Project Phase 6 (CMIP6) experimental design and organization. *Geosci. Model Dev.* **9**, 1937–1958 (2016).
- O'Neill, B. C. et al. The Scenario Model Intercomparison Project (ScenarioMIP) for CMIP6. *Geosci. Model Dev.* **9**, 3461–3482 (2016).

48. Kim, H. Global Soil Wetness Project Phase 3 Atmospheric Boundary Conditions (Experiment 1) [Data set]. Data Integration and Analysis System (DIAS), <https://doi.org/10.20783/DIAS.501> (2017).
49. Zheng, F., Li, J., Ding, R. & Feng, J. Cross-Seasonal Influence of the SAM on Southern Hemisphere Extratropical SST and its Relationship with Meridional Circulation in CMIP5 models. *Int. J. Climatol.* **38**, 1499–1519 (2018).
50. Livezey, R. E. & Chen, W. Y. Statistical field significance and its determination by Monte Carlo techniques. *Month. Weath. Rev.* **111**, 46–59 (1983).
51. Nemani, R. R. et al. Climate-driven increases in global terrestrial net primary production from 1982 to 1999. *Science* **300**, 1560–1563 (2003).
52. Kim, J. S., Kug, J. S. & Jeong, S. J. Intensification of terrestrial carbon cycle related to El Niño-Southern Oscillation under greenhouse warming. *Nat. Commun.* **8**, 1674 (2017).

Acknowledgements

J.-S.Kim and G.S.-S. were supported by the University of Zurich research priority program on Global Change and Biodiversity (URPP GCB). J.-S.Kug was supported by the R&D Program for Oceans and Polar Regions of the National Research Foundation (NRF) funded by the Ministry of Science and ICT (2020M1A5A1110670). S.J. was supported by the R&D Program for Oceans and Polar Regions of the National Research Foundation (NRF) funded by the Ministry of Science and ICT (NRF-2020M1A5A1110493). J.-H.Y. was supported by the National Research Foundation (NRF-2020M1A5A1110578). N.Z. was supported by NOAA Climate Program Office (grant number: NA18OAR4310266) and NIST Greenhouse Gas Measurement Program (70NANB14H333). Y.Z. and X.C. were supported by the National Natural Science Foundation of China under Grant Nos.41771049 and China Scholarship Council. M.W. was supported by the UK National Centre for Earth Observation. K.I. was supported by JSPS KAKENHI Grant Number JP19H05668. Phenological datasets were provided by the meteorological information center of the China Meteorological Administration (CMA), Korea Meteorological Administration (KMA) and Japan Meteorological Agency (JMA). Community Land surface Model version 5 (CLM5) simulations were performed on the Piz Daint supercomputer at the Swiss National Supercomputing Centre (CSCS) under project ID uzh28.

Author contributions

J.-S.Kim compiled the data, conducted analyses, prepared figures, and wrote the manuscript. J.-S.Kim and J.-S.Kug designed the research and wrote the majority of the manuscript content. J-HY and NZ provided the source code of the VEGAS model. YZ

and XC conducted and analysed phenology datasets in China. KI provided the data-driven estimates of terrestrial CO₂ fluxes across Asia. J.-S.Kim, J.-S.Kug, SJ, J-HY, NZ, JH, J-HJ, YZ, XC, MW, KI, and GS-S discussed the results and wrote the manuscript.

Competing interests

The authors declare no competing interests.

Additional information

Supplementary information The online version contains supplementary material available at <https://doi.org/10.1038/s43247-022-00343-7>.

Correspondence and requests for materials should be addressed to Jong-Seong Kug.

Peer review information *Communications Earth & Environment* thanks Shilong Piao and the other, anonymous, reviewer(s) for their contribution to the peer review of this work. Primary Handling Editors: Joy Merwin Monteiro and Clare Davis. Peer reviewer reports are available.

Reprints and permission information is available at <http://www.nature.com/reprints>

Publisher's note Springer Nature remains neutral with regard to jurisdictional claims in published maps and institutional affiliations.



Open Access This article is licensed under a Creative Commons Attribution 4.0 International License, which permits use, sharing, adaptation, distribution and reproduction in any medium or format, as long as you give appropriate credit to the original author(s) and the source, provide a link to the Creative Commons license, and indicate if changes were made. The images or other third party material in this article are included in the article's Creative Commons license, unless indicated otherwise in a credit line to the material. If material is not included in the article's Creative Commons license and your intended use is not permitted by statutory regulation or exceeds the permitted use, you will need to obtain permission directly from the copyright holder. To view a copy of this license, visit <http://creativecommons.org/licenses/by/4.0/>.

© The Author(s) 2022